THE JOURNAL OF PHYSICAL CHEMISTRY B

Article

pubs.acs.org/JPCB

Effect of Electric Field Orientation on the Mechanical and Electrical Properties of Water Ices: An Ab-initio Study

Giuseppe Cassone,[†,‡,§,∥,⊥] Paolo V. Giaquinta,[†,#] Franz Saija,[*,‡] and A. Marco Saitta[§,∥,¶]

[†]Dipartimento di Fisica e di Scienze della Terra, Università degli Studi di Messina, Contrada Papardo, 98166 Messina, Italy

[‡]CNR-IPCF, Viale Ferdinando Stagno d'Alcontres 37, 98158 Messina, Italy

[§]UMR 7590, IMPMC, UPMC Univ Paris 06, Sorbonne Universités, F-75005 Paris, France

[∥]UMR 7590, IMPMC, CNRS, F-75005 Paris, France

ABSTRACT: We present a first-principles study of the properties of ordinary hexagonal ice (phase I_h) and of its proton-ordered version (phase XI) under the action of static electric fields. We compute the mechanical response to the field in addition to the ionic current−voltage diagrams; we also analyze several other microscopic aspects of the proton transfer mechanism, with particular emphasis on the role played by the oxygen sublattice in driving molecular dissociation. We further study the topological aspects of the mechanical and electrical responses by orienting the external field along two different crystalline directions in both ice samples. At variance with ice I_h, ice XI displays an anisotropic behavior in the range of explored field intensities. In fact, when the direction of the field coincides with the ferroelectric axis, sustained molecular dissociation and proton transfer events are both observed just beyond a given field intensity; instead, the two processes exhibit different activation thresholds when the field is oriented along another symmetry axis. The underlying mechanism of molecular dissociation appears to be the same in solid and liquid water independently of the direction of the field.

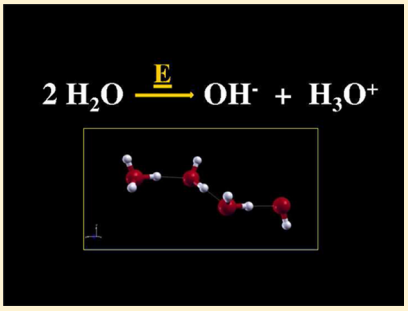

I. INTRODUCTION

Water is for some aspects one of the simplest molecules in nature but several of its properties are not yet fully understood, mainly because of the subtle role played by hydrogen bonds (H-bonds). In addition to the vast and still highly debated phenomenology exhibited by stable and metastable liquid water,[1] even the thermodynamics of its solid forms is rather baroque in that the phase diagram includes at least 16 crystalline structures.[2] At ambient conditions the stable solid phase is ice I_h, in which molecules are located on the sites of a hexagonal lattice while being orientationally disordered (i.e., the proton sublattice is randomly distributed). By cooling KOH-doped ice I_h down to a temperature of 72 K, one obtains ice XI, the proton-ordered counterpart of ice I_h,[3,4] in which the dipole moment of each molecule is mainly oriented along the *c*-axis, its *z*-component thus being everywhere positive in the standard lattice. In the ice I_h to ice XI first-order phase transition the hydroxide ions of KOH catalyze the rearrangement of H-bonds via the formation of defects which lead to an improved molecular mobility. In this way the molecules find a more stable arrangement by reducing the symmetry of the phase from $P6_3/mmc$ to $Cmc2_1$, thus giving rise to the ferroelectric phase known as ice XI. The ordering of the proton sublattice also affects many important properties of the material, such as its electrical polarizability and conductivity. Actually, ice can be described as a "protonic semiconductor" and the understanding of its electrical behavior is highly relevant for even more complex systems and materials in which proton transfer (PT) takes place along H-bonded chains.

In liquid water the process through which a H_2O molecule dissociates, thus setting the acid or basic character (pH) of an aqueous solution, is known as *protolysis* and occurs according to the reaction

$$2H_2O \rightleftharpoons OH^- + H_3O^+ \quad (1)$$

in which, formally, a PT occurs between two water molecules. This is an extremely rare event at standard conditions, both in liquid and in solid water, as can be argued from their respective pH values. However, by applying an external electric field, it is possible to stimulate in a systematic fashion the molecular dissociation process and, eventually, to obtain an effective protonic current via correlated proton jumps which take place along H-bonded chains.

In ice phases, hydronium and hydroxide ionic defects are responsible, together with Bjerrum (i.e., orientational) defects, for electrical transport processes.[2] Although the underlying microscopic motions that lead to the fast transport rate of H_3O^+ have been known since the 1800s as the Grotthuss mechanism,[5] a satisfactory and coherent theoretical framework which may explain the complex processes associated with PT through point defects in aqueous systems is still missing.

Recently, great effort has been made to fill the gap between theory and experimental observations,[6−10] also in relation to the transformation of proton-disordered systems into proton-

Received: July 23, 2014
Revised: September 23, 2014
Published: September 29, 2014

ordered systems under the effect of electric fields.[11] In a recent work we performed ab initio numerical calculations of the static and dynamical properties involved in molecular dissociation and PT in ices I_h and XI.[12]

To shed more light on this apparently elaborate phenomenon, we present in this manuscript a series of novel ab initio simulations that are performed to understand and exploit the symmetry differences between ice I_h and ice XI. This aim is achieved by applying a static electric field along two different crystalline directions. Upon monitoring and analyzing the PT activity in the two topologically different materials, important conclusions can be drawn. This kind of analysis is of paramount importance because the hydrogen migration properties are relevant in many disparate fields[13] and the related (an)isotropic piezoelectric effects are important[14] also for H-bonded systems.[15] We investigate several dynamical aspects of the H-bond structure during the proton migration process, which can be compared with the similar mechanism in liquid water. In this way it is possible to obtain a more exhaustive comprehension of the mechanical and electrical responses of ice I_h and ice XI subject to the action of a static electrical perturbation.

The manuscript is structured as follows. In section II we illustrate the methodology of our investigation; in section III we discuss our results for the mechanical and electrical properties of the two materials. Section IV is finally devoted to concluding remarks.

II. THEORY AND SIMULATION

The ab initio calculations presented here are performed by using the software package Quantum ESPRESSO,[16] based on the Car–Parrinello approach.[17] Samples of ice I_h, whose structure belongs to the $P6_3/mmc$ space group, and of its proton-ordered counterpart ice XI, which instead falls in the $Cmc2_1$ space group, are investigated under the action of intense electric fields applied along two directions, viz., the *c*-axis and the *b*-axis, to study the phenomenon of ionic conduction. The implementation of an external field in density functional theory (DFT) codes can be achieved by exploiting the modern theory of polarization based on Berry's phases,[18] as done in ref 19. Our samples contain 64 H_2O molecules arranged in an orthorhombic cell with parameters a = 9.05 Å, b = 15.67 Å, and c = 14.87 Å. The potential relevance of size effects was already discussed in a recent paper by considering samples composed of 96 and 128 molecules;[12] it turned out that the size of the samples does not significantly affect the qualitative aspects of the electrical behavior of the investigated systems. As usual, the structures are replicated in space by using periodic boundary conditions (PBCs). The oxygen sublattices are identical in the two crystalline structures;[4,20] however, the arrangements of the hydrogen atoms differ significantly. In fact, the orientations of the molecules in ice I_h, though complying with the Bernal–Fowler ice rules,[21] are distributed in a random way, at variance with ice XI where they are in fact ordered.

We carry out ab initio simulations at the nominal temperature of 300 K which, according to the literature,[22−24] should provide a good description of the structural properties of water systems at a temperature of about 250 K. The explored range of electric field intensities has its maximum at 0.36 V/Å, and it has been reached with a step increment of about 0.03 V/Å. For each value of the field, we run the dynamics for about 2 ps, accumulating a total simulation time longer than 20 ps for each sample and field direction. The fictitious electronic mass is set to a value of 300 au, with a cutoff energy of 35 Ry and a cutoff energy for the charge density of 280 Ry. With such values, the samples are described in a realistic way because the core electronic interaction is being depicted through ultrasoft pseudopotentials (USPPs). Moreover, the exchange and correlation functional used in our code is the Perdew–Burke–Ernzerhof (PBE) functional,[25] which belongs to the generalized gradient approximation (GGA) class. This functional turns out to be a dependable tool for systems in the currently investigated thermodynamic conditions[26−28] and under the effect of static electric fields.[29] However, in the light of some recent debate on its reliability for aqueous systems,[30−32] we carry out some calculations with the BLYP functional[33] as well.

The dynamics of ions is carried out in the constant number, volume, and temperature (*NVT*) ensemble, by using the Verlet algorithm and a Nosé–Hoover thermostat set at a frequency of 13.5 THz.

The energies of the distorted structures and the corresponding equations of state (EOS) are also calculated using the same DFT-based Quantum ESPRESSO code. Following the energy-strain approach, we execute a series of relaxation simulations by using the steepest-descent technique combined with the damping dynamics of the ions for different values of the cell parameters, while keeping the cell volume fixed over the whole range of explored field strengths. With this approach it is also possible to calculate, inter alia, the c_{66} component of the stiffness tensor (i.e., one of the elastic constants), that is related to the curvature of the EOS around its minimum. In hexagonal systems only five stiffness constants are independent, viz., c_{11}, c_{12}, c_{13}, c_{33}, and c_{44}, because $c_{66} = {}^1/_2(c_{11} - c_{12})$.[34] It is possible to determine this latter quantity through the relation (expressed here in the Voigt matrix notation)

$$c_{66} = \frac{1}{V}\frac{\partial^2 E}{\partial \varepsilon_6 \partial \varepsilon_6}\bigg|_{E=E_0} \tag{2}$$

where V is the volume, ε denotes an infinitesimal deformation, and E is the self-consistent total energy of the system. In practice, the derivative is carried out on a quadratic fit of the data for the energy.

III. RESULTS

A. Mechanical Properties. To evaluate the equation of state (EOS), we perform a series of relaxation simulations by applying the field along the *c*-axis in ices I_h and XI, and along the *b*-axis in the proton-ordered structure only. In this way we obtain the energy profiles versus deformation over the range of the explored field intensities that are shown in Figure 1. In ice XI, when the field is oriented along the *c*-axis, upon increasing the field strength the minimum of the energy shifts to lower values of the ratio between the cell parameters *c* and *a* (Figure 1a); instead, no shift at all is observed in the I_h phase (Figure 1b) or when the field is oriented along the *b*-axis of the ferroelectric sample (Figure 1c). However, the most significant difference is found in the curvature: in ice XI the shape of the EOS changes with the field strength when the field is oriented along the *c*-axis, a behavior that, instead, is not exhibited by ice I_h as well as by ice XI under the effect of a field parallel to the *b*-axis.

Figure 2 shows the elastic constant c_{66}, plotted as a function of the field intensity; in ice I_h the value of this quantity computed for vanishing electric field (1.9 GPa) turns out to be lower than both the available experimental results[2,35,36] and

dx.doi.org/10.1021/jp507376v | J. Phys. Chem. B 2014, 118, 12717−12724

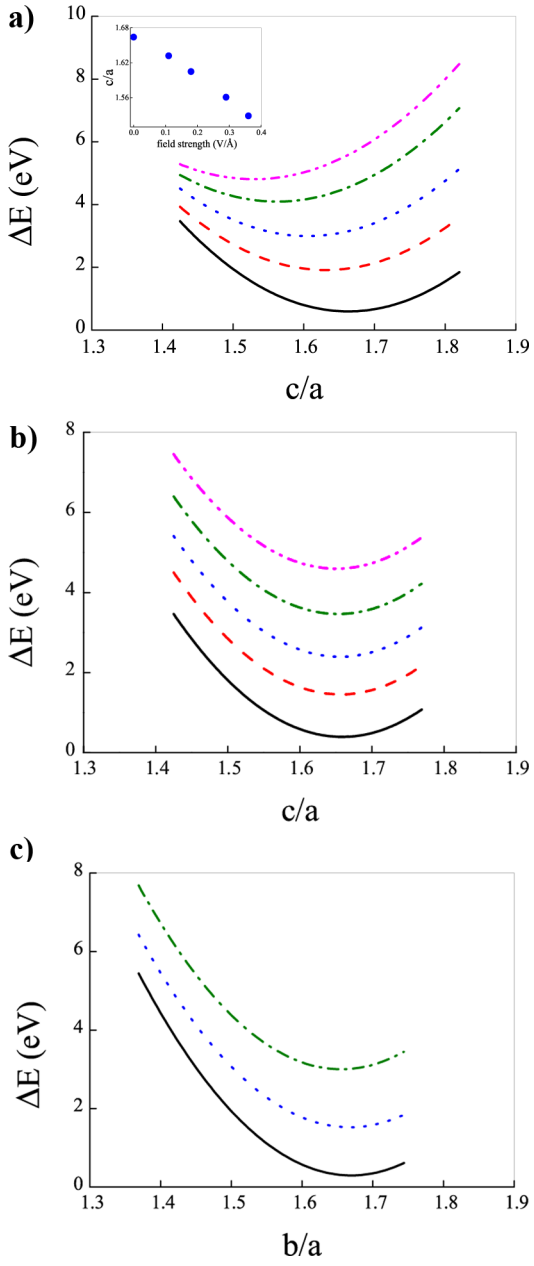

Figure 1. Equations of state (EOS) for various field intensities. (a) ice XI under the action of a field oriented along the *c*-axis. Note the change of the curvature and the shift of the minimum toward lower values of the ratio *c*/*a* as the intensity of the field increases. In the inset we plot the value of *c*/*a*, which minimizes the energy as a function of the field strength. (b) Ice I_h. The curvature is almost independent of the field. (c) Ice XI under the action of a field oriented along the *b*-axis. Note that the curvature does not change with the field strength. Black lines correspond to the vanishing field cases; red dashed lines, blue dotted lines, green dot-dashed lines, and magenta dot-dot-dashed lines refer to field strengths 0.11, 0.18, 0.29, and 0.36 V/Å, respectively. Each curve is rigidly shifted in energy for clarity.

another independent theoretical estimate[37] by about 1.5 GPa. A manifestly different behavior is observed in the two crystalline structures: in ice I_h the elastic constant c_{66} shows a weak dependence on the field strength, whereas in ice XI it actually decreases with the field intensity in a linear way. This difference is ultimately related to the structural symmetries. The proton-ordered sublattice of ice XI allows for an enhanced coupling

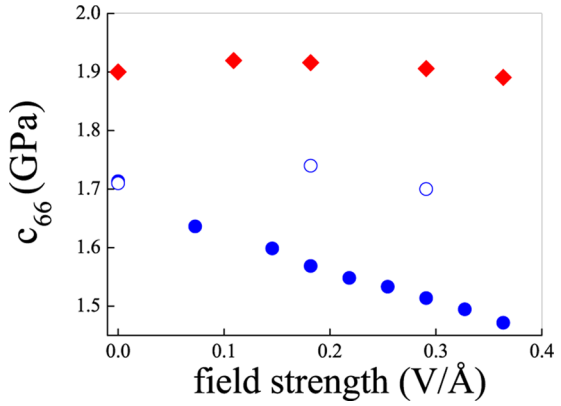

Figure 2. c_{66} element of the stiffness tensor plotted as a function of the electric field intensity. Red diamonds and blue solid circles refer to the case of an electric field oriented along the *c*-axis of ice I_h and ice XI, respectively; blue open circles refer to the case in which the electric field is oriented along the *b*-axis of ice XI.

between the molecular dipole moments and the external field when this is oriented along the ferroelectric axis. It turns out that this circumstance makes the system softer by forcing a partial molecular alignment along the field direction. In the cases of ice I_h subject to a field along the *c*-axis and of ice XI under the effect of an electric field acting along the *b*-cell parameter direction, the coupling of the local molecular dipole moments with the external field is not as straightforward; the different distributions of dipole moments, whose projection onto the field direction varies from negative to positive values, prevent a softening of the two structures because a conspicuous molecular reorientation of the dipoles is impossible in the mentioned crystalline phases during the relaxation experiment. We finally note that the dielectric constants of the two samples, when calculated with the PBE and with other exchange and correlation functionals,[38−40] exhibit very similar values; hence, we may argue that they do not influence in an appreciable way the ambivalent behavior of the mechanical response discussed above.

B. Electrical Properties. In a recent work we had already presented a series of results about the proton static conductivities of ices I_h and XI under the action of an external electric field oriented along the *c*-axis [001] direction.[12] We interpreted the differences in the respective dissociation and current thresholds by considering the different orientational distributions of the water molecules in the two crystalline structures. In addition, we explained the resulting static conductivities through the percent fractions of field-induced defects. Here we want to discuss the intrinsic electrical anisotropy that is due to the proton arrangements by orienting the electric field along another direction of the crystal, i.e., the *b*-axis [010] direction, in the common hexagonal phase of ice as well as in its proton-ordered counterpart. The close correspondence of the dissociation (0.25 V/Å) and current (0.36 V/Å) thresholds in ice I_h and liquid water[29,41] was explained through the similarity of the distributions of dipole moments in the two phases.

However, in the proton-ordered case we found substantially similar threshold values of the field strength for both processes of molecular dissociation and sustained proton diffusion (0.18−0.22 V/Å). We noted that these latter estimates fall in a range of values lower than those found in ice I_h and liquid water as a consequence of the enhanced coupling between the external

dx.doi.org/10.1021/jp507376v | J. Phys. Chem. B 2014, 118, 12717−12724

field and the dipole moments; moreover, because the polarization effects are more important in the ferroelectric case, the local electrical environment enhances the probability of molecular dissociation and protonic diffusion along the field direction, thus giving rise to a single-threshold process, at variance with the I_h and liquid water cases. The PT mechanism occurs along a sequence of H-bonds until a proton has traveled a certain path that becomes infertile as for the transfer of another proton. The reactivation of a given proton transmitting H-bonds passage is achieved via the formation of Bjerrum defects.[2,42]

Upon orienting the external electric field along the *b*-axis direction, it is possible to compare and understand the coupling between dipole moments and the external electric field, thus obtaining partial insights on the time-dependent local polarization effects. On account of the quasi-random molecular orientation distribution in common ice, one would expect a Cartesian axis reversal invariance with respect to a change in the field propagation direction. However, in the ferroelectric phase, a different coupling, as compared with the case shortly described above (electric field along the ferroelectric axis), arises from the intrinsic electrical anisotropy of the material.[3,4,20]

These predictions are confirmed by the present simulations. In fact, in ice I_h no sensible change is found in the molecular dissociation and sustained proton diffusion threshold values, for any orientation of the field; instead, in the ice XI samples these thresholds are modified in a sensitive way and a two-stage process takes place.

In ordinary ice the ionization event becomes manifest for 0.22 V/Å, but a net proton flow occurs for field intensities of 0.32−0.36 V/Å. We note that, notwithstanding the fact that a net proton flow can be measured for a field strength of about 0.32 V/Å, the discrepancy with the result obtained after orienting the field along the *c*-axis falls within the error of our calculations; moreover, this discrepancy can be related to the small enhancement of the dielectric anisotropy introduced by the DFT exchange and correlation functional used.[43]

The field strength threshold of the dissociation events in ice XI is also registered, somewhat surprisingly, for 0.22 V/Å, but the most favorable circumstance after molecular dissociation is the rattling of the proton shared between the two forming ions, and only for an intensity of 0.29 V/Å do we observe the first net proton flow events. This two-stage process is the first neat alteration of the response behavior as compared to the case in which the field direction is parallel to the ferroelectric axis. We also note that the corresponding molecular dissociation thresholds in the simulations carried out with the BLYP functional are 0.25 and 0.22−0.25 V/Å for ice I_h and ice XI, respectively. Differences with respect to the PBE results fall within the error range of our calculations, and the estimates of protonic current thresholds are the same for the two functionals.

1. Dynamics of H-Bond Chains. With regard to the local dynamics, when the dissociation events occur, we observe a shortening of the H-bond lengths that allows for a fast PT along the respective reaction coordinates, as shown in Figure 3 for the two crystalline phases. In the ice XI case the average oxygen−oxygen distances are slightly shorter than in the hexagonal common phase, which suggests a more efficient transfer process of defects.

We define the H-bond wire length as the sum of the individual donor−acceptor distances between H-bond connected oxygen atoms in which a molecular dissociation has occurred. Figure 4a shows the behavior of an ice I_h H-bond wire, whose length has been rescaled by dividing it by the number of involved intermolecular distances and in which a combined PT between the oxygens has occurred in a few hundreds of femtoseconds, followed by a ready proton

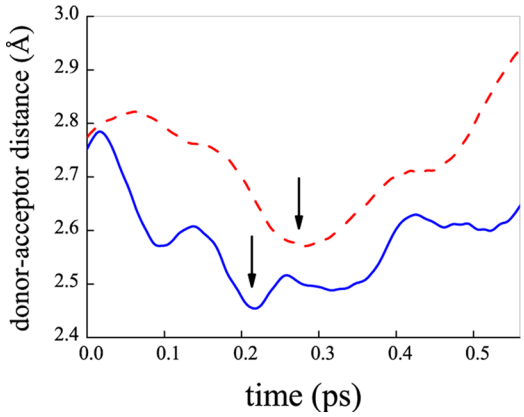

Figure 3. Donor−acceptor distance between two molecules measured on the occasion of the first molecular dissociation events when the field is oriented along the *b*-axis of ice I_h (red dashed line) and of ice XI (blue solid line). The instant at which the ionization occurs is signaled by the arrow.

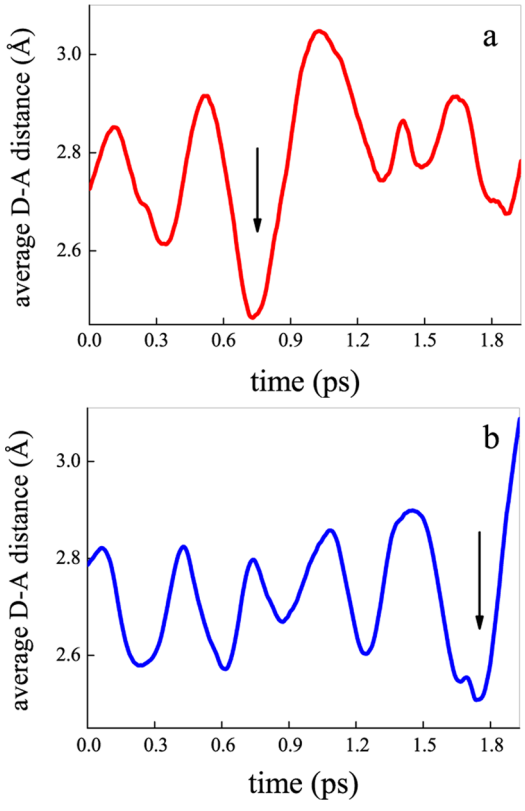

Figure 4. (a) Average donor−acceptor distances of an H-bond chain of ice I_h in which the first dissociation events occur for E = 0.22 V/Å. The process is signaled by the absolute minimum pointed by the arrow. (b) Average molecular distances in an H-bond wire in ice XI under the action of a field oriented along the *c*-axis and in which the first dissociation events occur for E = 0.18 V/Å. The intermolecular length shows a huge increment after attaining its absolute minimum.

dx.doi.org/10.1021/jp507376v | J. Phys. Chem. B 2014, 118, 12717−12724

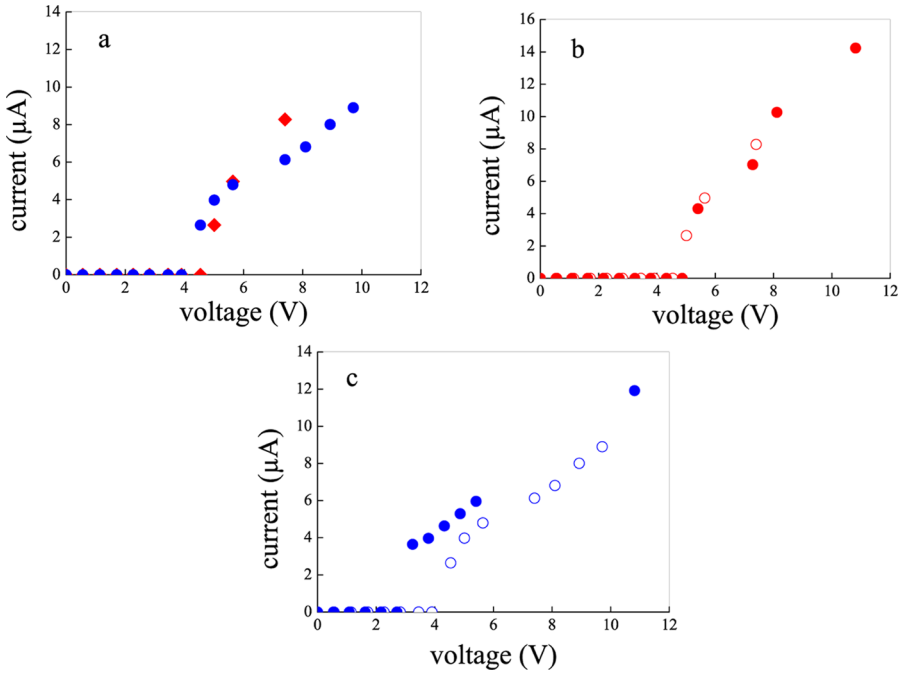

Figure 5. (a) Ionic current−voltage diagrams corresponding to a field oriented along the cell parameter b = 15.67 Å;. Red solid diamonds refer to a sample of ice I_h; blue solid circles refer to a sample of ice XI. (b) Ionic current−voltage diagrams of ice I_h under the action of a field oriented along the b-axis (red open circles) and the c-axis (red solid circles). (c) Ionic current−voltage diagrams of ice XI under the action of a field oriented along the b-axis (blue open circles) and the c-axis (blue solid circles).

recombination. A pronounced relative minimum is visible just before the global one, indicating a first (unsuccessful) attempt at molecular dissociation and local PT. We observe another curious aspect that characterizes all the investigated H-bond wires: after dissociation, the length of the "wire" always increases with respect to the average one and attains a global maximum just after the global minimum, showing a sort of chain "breath"; in all cases (even in the ferroelectric one-stage mechanism of PT shown in Figure 4b) subsequent correlated molecular dissociations, produced immediately later along the *same* H-bond path, do not occur. This finding is consistent with the Jaccard theory of defects propagation.[42] Hence, we argue that the mechanism underlying molecular dissociation, which implies a certain degree of cooperation between the oxygen atoms, is the same in liquid water[6,44] as well as in the crystalline phases that we have investigated.

2. Ice I_h vs Ice XI: Anisotropy Effects. As already noted, the field intensity value that allows for a sustained protonic current in common ice is comparable to that observed in liquid water (0.36 V/Å)[12,29,41] and does not substantially depend on the field direction. The response of ice I_h to static electrical perturbations is intrinsically isotropic on account of the topological isotropy conferred to this ice phase by its proton sublattice. Incidentally, this result recalls the hypothesized isotropic nature of the G correlation parameter (also known as dipolar autocorrelation coefficient) in ice I_h; this finding is also supported by Monte Carlo simulations and is intimately related to the electrical response via the dipole moments distribution.[45]

However, when the field is oriented along the b-axis of ice XI, the behavior of the material changes significantly if compared with that of the same structure under an electric field oriented along the c-axis. In these conditions the molecular dissociation events and the subsequent proton diffusion are not simultaneous, as previously noticed for ice XI under the action of a field parallel to the ferroelectric direction. In particular, as the concentration of both types of defects becomes relevant, the system starts to conduct in almost the same way as in the case of ice XI when the field lies along the ferroelectric axis, evolving, from a certain point of view, to a partial (unstable and field-induced) ferroelectricity.

To give a more complete description of the ionic conduction in these systems, we also calculate the ionic current−voltage diagrams corresponding to our unit cells. The results are displayed in Figure 5a for the two phases when the electric field is oriented along the b-axis; parts b and c of Figure 5 show the comparison with the previously investigated cases where the field is oriented along the c-axis for ice I_h and XI, respectively.[12] All the ionic current−voltage diagrams show a ohmic behavior after a net PT process has taken place. These results confirm those found in several experiments performed on ice I_h samples.[46,47] It is not surprising to observe a good agreement between the two different situations (Figure 5b); a similar conclusion follows from the calculations performed with the BLYP functional. However, as far as ice XI is concerned, we observe a different behavior below the current threshold value (Figure 5c). This result can be interpreted at relatively low voltages (up to about 5 V for our unit cell) by considering that the system under the action of a field oriented along the b-axis, generates a sufficient concentration of defects, up to a field strength of 0.29 V/Å (ionic current threshold). Above this value, the sample is somewhat indistinguishable, as for the electrical response, from a similar sample under the effect of an electric field acting along the ferroelectric axis. The hypothetic slight differences in the derivatives (i.e., in the conductivities) of the respective ionic current−voltage diagrams do actually fall within the error bars of our calculations. The reliability of the present estimate for the current intensity flowing in ice XI at the current threshold is confirmed by the equivalent results obtained with the BLYP functional.

dx.doi.org/10.1021/jp507376v | J. Phys. Chem. B 2014, 118, 12717−12724

3. Partial Ferroelectricity along the b-Axis of Ice XI. When a sample of ice XI is subject to a field strength equal to or greater than 0.29 V/Å along the *b*-axis, it is possible to observe a sort of partially ferroelectric domain along the field axis in the presence of a conspicuous amount of defects. The process can be explained as follows: starting from the symmetry of the dipole moments distribution of the ice XI molecular structure, one can observe that there are some planes (as the middle plane almost parallel to the *xy* plane in the orthorhombic centered unit cell shown in Figure 6) in which molecules (3- and 4-type in Figure 6) are hosted that exhibit a large positive *y*-component of dipole moments. In the absence of the field, this component falls in a ranges 2.51−2.69 and 2.90−3.10 D for the 3- and 4-type molecules shown in Figure 6, respectively.[48,49] One half of the ice XI planes are ferroelectric with respect to the *b*-axis direction, and the remaining ones are antiferroelectric.

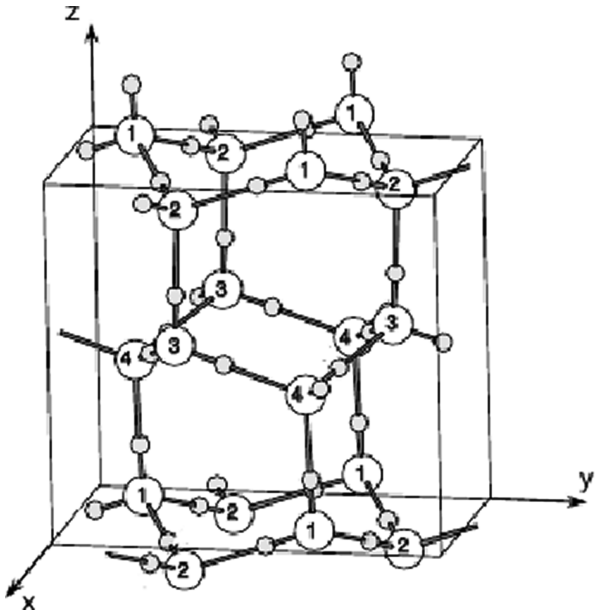

Figure 6. $Cmc2_1$ ice XI orthorhombic centered unit cell. Partially modified Figure 1 reprinted with permission from ref 4. Copyright 2004 American Physical Society.

Also ice I_h has a certain number of molecules that are mostly oriented along the *b*-axis with a similar *y*-component of their dipole moment as reported above, but there are only *triplets* of connected molecules with this peculiarity, whose chain extremities are H-bonded to other chains of H-bonded molecules that consistently exhibit lower (and in most cases negative) *y*-components of their dipole moments, and so on. In this way, when a field is applied along any direction, the surrounding environment prevents any potential ferroelectric transition in the common ice phase, even for high field intensities.

These observations become crucial when a static electric field is applied along the *b*-axis. In fact, the first molecules that start to dissociate in ice XI are those belonging to the planes mentioned above and, as the concentration of defects increases with the external field intensity, the system develops a partial ferroelectricity along the Hamiltonian discontinuity axis along which the field is oriented. This behavior is likely due to the collective positive dipole moment (with respect to the field direction) exhibited by these planes, which is enhanced by the field itself. This leads, in turn, to an enhancement of the local electric field, which produces more and more defects and, correspondingly, favors a larger molecular mobility. These circumstances are accompanied by a shortening of the transition time.[3] It is also known that the H-bond network is slightly distorted by defects.[2] The H-bonds that lie transversal to the field direction get weaker and weaker as the field intensity increases.[50] All these considerations justify the fact that the molecules have the opportunity of slightly rotating around the more robust H-bond, making a statistical attempt at the formation of Bjerrum defects. The creation of ionic propagating defects, beyond the current threshold, is not by itself sufficient to explain the ionic conductivity. The formation of Bjerrum defects is crucial in that they can "open" new protonic paths along H-bonds[2,42] after an ion has diffused away. The propagation of defects takes place via the Grotthuss mechanism.[5]

Summing up, different pieces of evidence, such as the basic PT mechanism, the field-induced enhancement of molecular mobility, the generation of ionic defects, and the stronger local polarization effects created in one-half of the *ab* planes, make the formation of ferroelectric patches possible in ice XI under the effect of an electric field with a strength larger than 0.29 V/Å and projected along the *b*-axis.

This phase is obviously different from the standard ice XI structure, as one can see from the distribution of H-bonds (i.e., the symmetry along the *b*-axis is different from the symmetry along the *c*-axis). However, when the problem is seen simply from the electrical point of view, the two conductors are practically the same. In fact, also in the ice XI case subject to a field along the *c*-axis and above the current threshold, it is possible to find molecular configurations in which molecules are obviously present that have a negative *z*-component of the dipole moment just after/before being involved in PT: this behavior is inherent to the conduction process generated by protonic defects.

It is important to remark that a complete ferroelectric phase transition is impossible; in fact, in such a case, the system would melt because of the formation of alternating series of D- and L-defects between those planes that we have formerly called ferroelectric and antiferroelectric (with respect to the *b*-axis) (Figure 7). Moreover, the condition of partial ferroelectricity is only a nonequilibrium situation induced by the field and by the related conspicuous amount of defects (Figure 8). Because of the formation of defects and their propagation via field interactions, one can argue that the conduction properties of ice XI are very similar to those discussed in the two cases in which a field along the ferroelectric axis or along the *b* one is involved, provided that the current threshold of the latter has

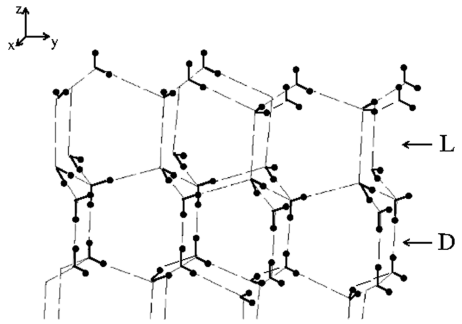

Figure 7. "Impossible" ferroelectric phase (along the *b*-axis) of ice XI.

dx.doi.org/10.1021/jp507376v | J. Phys. Chem. B 2014, 118, 12717−12724

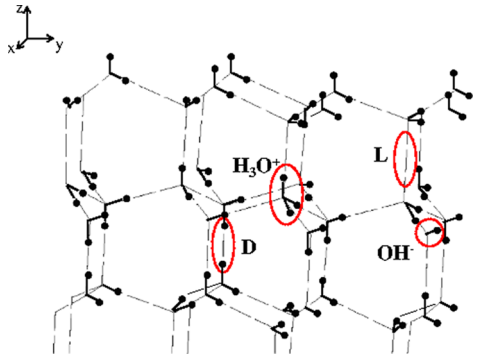

Figure 8. A realistic sketch, without H-bond perturbations, of the molecular arrangement when an electric field stronger than 0.29 V/Å is applied along the *b*-axis of ice XI. Some molecules are not shown.

been reached and overcome. This finding is not particularly striking if one imagines that also in a ferroelectric sample under the effect of a field parallel to the *c*-axis at some instants some molecules are oriented oppositely with respect to the field to eventually "open" some H-bond paths for another PT or to "close" them after a PT has taken place along a given path.

IV. CONCLUSIONS

In this work we have investigated some aspects concerning the dynamics of the proton transfer mechanism in ice I_h and ice XI, under the action of a static electric field that has been oriented along two different directions in both samples. After obtaining the equation of state, we have calculated the mechanical response through the stiffness tensor. We notice that it does not depend of the field intensity (at least, in the investigated regime) when the field is applied along the *c*-axis of the I_h phase. Moreover, also ice XI shows the same trend when the field is oriented along the *b*-axis. This is no longer true when the field is parallel to the ferroelectric axis. In fact, a monotonic decrease of the elastic constant c_{66} has been observed when the field intensity increases, which suggests a softening of the structure.

In addition to the mechanical behavior of the samples, we also have focused on their electrical responses. In a previous work we had noticed several important common aspects shared by the proton-disordered solid phase of water and the liquid phase, such as the thresholds of molecular dissociation and protonic current.[12]

As far as the ice XI is concerned, as expected from its intrinsic anisotropy, some differences are observed when different directions of the external field are chosen. In particular, the one-stage mechanism, involving at the same time molecular dissociation and proton transfer, observed when the field direction coincides with the ferroelectric axis, disappears when the field is oriented along another axis (e.g., the *b*-axis), in which case the process develops in two stages. Moreover, for high field strengths dipole moments tend to align with the field in ice XI more easily than in the I_h phase because of the ferroelectric nature exhibited by many of its planes along the *b*-axis direction. This pseudoferroelectricity is enhanced and propagated by field-induced defects formation.

A significant finding of this study is the acquisition that the underlying mechanism of molecular dissociation is substantially the same in liquid as well as in solid water, involving a high degree of cooperation of the oxygen sublattice. The dynamics of the molecules is characterized by a compression of the H-bond wires that participate in the dissociation events, independently of the symmetry of the system. Another common feature shared by all the investigated systems is the increase of the length of the H-bond chain that immediately follows its compression, a circumstance that prevents the transfer of a proton along the same path.

AUTHOR INFORMATION

Corresponding Author

*F. Saija. E-mail: franz.saija@cnr.it.

Notes

The authors declare no competing financial interest.

⊥G. Cassone. E-mail: giuseppe.cassone@impmc.upmc.fr.

#P. V. Giaquinta. E-mail: paolo.giaquinta@unime.it

¶A. M. Saitta. E-mail: marco.saitta@impmc.upmc.fr.

ACKNOWLEDGMENTS

We acknowledge the UPMC Mesocenter and the French GENCI/IDRIS Supercomputing Facility for CPU time (x2014091387). G.C. and A.M.S. thank Prof. S. Savasta for his support. G.C. thanks M. S. Cassone for the graphical assistance.

REFERENCES

(1) Debenedetti, P. G. *Metastable Liquids - Concepts and Principles*; Princeton University Press: Princeton, NJ, 1996.

(2) Petrenko, V. F.; Whitworth, R. W. *Physics of Ice*; Oxford University Press: Oxford, U.K., 1999.

(3) Tajima, Y.; Matsuo, T.; Suga, H. Phase Transition in KOH-Doped Hexagonal Ice. *Nature* **1982**, *299*, 810−812.

(4) Umemoto, K.; Wentzcovitch, R. M.; Baroni, S.; de Gironcoli, S. Anomalous Pressure-Induced Transition(s) in Ice XI. *Phys. Rev. Lett.* **2004**, *92*, 105502.

(5) Grotthuss, C. J. T. Sur la Décomposition de l'Eau et des Corps qu'elle Tient en Dissolution à l'aide de l'électricité galvanique. *Ann. Chim.* **1806**, (Paris) LVIII, 54−74.

(6) Hassanali, A.; Giberti, F.; Cuny, J.; Kühne, T. D.; Parrinello, M. Proton Transfer Through the Water Gossamer. *Proc. Natl. Acad. Sci. U. S. A.* **2013**, *110*, 13723−13728.

(7) Cwiklik, L.; Buch, V. Hydroxide Trapped in the Interior of Ice: a Computational Study. *Phys. Chem. Chem. Phys.* **2009**, *11*, 1294−1296.

(8) Tuckerman, M. E.; Chandra, A.; Marx, D. Structure and Dynamics of OH-(aq). *Acc. Chem. Res.* **2006**, *39*, 151−158.

(9) Dagrada, M.; Casula, M.; Saitta, A. M.; Sorella, S.; Mauri, F. Quantum Monte Carlo Study of the Protonated Water Dimer. *J. Chem. Theor. Comp.* **2014**, *10*, 1980−1993.

(10) Bronstein, Y.; Depondt, P.; Finocchi, F.; Saitta, A. M. Quantum-driven Phase Transition in Ice Described via an Efficient Langevin Approach. *Phys. Rev. B* **2014**, *89*, 214101.

(11) Zhao, H.; Kong, X.; Li, H.; Chang Jin, Y.; Long, L.; Cheng Zeng, X.; Huang, R.; Zheng, L. Transition from One-Dimensional Water to Ferroelectric Ice Within a Supramolecular Architecture. *Proc. Natl. Acad. Sci. U. S. A.* **2011**, *108*, 3481−3486.

(12) Cassone, G.; Giaquinta, P. V.; Saija, F.; Saitta, A. M. Proton Conduction in Water Ices under an Electric Field. *J. Phys. Chem. B* **2014**, *118*, 4419−4424.

(13) McIntosh, E. M.; Wikfeldt, K. T.; Ellis, J.; Michaelides, A.; Allison, W. Quantum Effects in the Diffusion of Hydrogen on Ru(0001). *J. Phys. Chem. Lett.* **2013**, *4*, i1565−1569.

(14) Bystrov, V. S.; Paramonova, E. V.; Bdikin, I. K.; Bystrova, A. V.; Pullar, R. C.; Kholkin, A. L. Molecular Modeling of the Piezoelectric Effect in the Ferroelectric Polymer Poly(vinylidene fluoride) (PVDF). *J. Mol. Model* **2013**, *19*, 3591−3602.

(15) Werling, K. A.; Griffin, M.; Hutchison, G. R.; Lambrecht, D. S. Piezoelectric Hydrogen Bonding: Computational Screening for a Design Rationale. *J. Phys. Chem. A* **2014**, *118*, 7404−7410.

(16) Giannozzi, P.; Baroni, S.; Bonini, N.; Calandra, M.; Car, R.; Cavazzoni, C.; Cesaroli, D.; Chiarotti, G. L.; Cococcioni, M.; Dabo, I.; et al. QUANTUM ESPRESSO: A Modular and Open-Source Software Project for Quantum Simulation of Materials. *J. Phys.: Condens. Matter* **2009**, *21*, 395502.
(17) Car, R.; Parrinello, M. Unified Approach for Molecular Dynamics and Density-Functional Theory. *Phys. Rev. Lett.* **1985**, *55*, 2471−2474.
(18) Berry, M. V. Quantal Phase Factors Accompanying Adiabatic Changes. *Proc. R. Soc. London A* **1984**, *392*, 45−57.
(19) Umari, P.; Pasquarello, A. *Ab initio* Molecular Dynamics in a Finite Homogeneous Electric Field. *Phys. Rev. Lett.* **2002**, *89*, 157602.
(20) Jackson, S. M.; Nield, V. M.; Whitworth, R. W.; Oguro, M.; Wilson, C. C. Thermally-Stimulated Depolarization Studies of the Ice XIIce Ih Phase Transition. *J. Phys. Chem. B* **1997**, *101*, 6177−6179.
(21) Bernal, J. D.; Fowler, R. H. A Theory of Water and Ionic Solution, with Particular Reference to Hydrogen and Hydroxyl Ions. *J. Chem. Phys.* **1933**, *1*, 515−548.
(22) Del Buono, G. S.; Rossky, P. J.; Schnitker, J. Model Dependence of Quantum Isotope Effects in Liquid Water. *J. Chem. Phys.* **1991**, *95*, 3728.
(23) Allesch, M.; Schwegler, E.; Gygi, F.; Galli, G. First Principles Simulations of Rigid Water. *J. Chem. Phys.* **2004**, *120*, 5192.
(24) Grossman, J. C.; Schwegler, E.; Draeger, E. W.; Gygi, F.; Galli, G. Towards an Assessment of the Accuracy of Density Functional Theory for First Principles Simulations of Water. *J. Chem. Phys.* **2004**, *120*, 300.
(25) Perdew, J. P.; Burke, K.; Ernzerhof, M. Generalized Gradient Approximation Made Simple. *Phys. Rev. Lett.* **1996**, *77*, 3865−3868; and *Phys. Rev. Lett.* **1997**, *78*, 1396.
(26) Fiolhais, C.; Nogueira, F.; Marques, M. *A Primer in Density Functional Theory*; Springer-Verlag: Berlin, Heidelberg, 2010.
(27) Santra, B. Density-Functional Theory Exchange-Correlation Functionals for Hydrogen Bonds in Water. *Ph.D. thesis*, 2010.
(28) Hamann, D. R. H_2O Hydrogen Bonding in Density-Functional Theory. *Phys. Rev. B* **1997**, *55*, R10157−R10160.
(29) Saitta, A. M.; Saija, F.; Giaquinta, P. V. *Ab initio* Molecular Dynamics Study of Dissociation of Water Under an Electric Field. *Phys. Rev. Lett.* **2012**, *108*, 207801.
(30) Santra, B.; Klimes, J.; Alfé, D.; Tkatchenko, A.; Slater, B.; Michaelides, A.; Car, R.; Sheffer, M. Hydrogen Bonds and van der Waals Forces in Ice at Ambient and High Pressure. *Phys. Rev. Lett.* **2011**, *107*, 185701.
(31) Morales, M. A.; Gergely, J. R.; McMinis, J.; McMahon, J. M.; Kim, J.; Ceperley, D. M. Quantum Monte Carlo Benchmark of Exchange-Correlation Functionals for Bulk Water. *J. Chem. Theor. Comp.* **2014**, *10*, 2355−2362.
(32) Alfè, D.; Bartók, A. P.; Csányi, G.; Gillan, M. J. Analyzing the Errors of DFT Approximations for Compressed Water Systems. *J. Chem. Phys.* **2014**, *141*, 014104−1 DOI: 10.1063/1.4885440.
(33) Becke, A. D. Density-Functional Exchange-Energy Approximation with Correct Asymptotic Behavior. *Phys. Rev. A* **1988**, *38*, 3098. Lee, C.; Yang, W.; Parr, R. Development of the Colle-Salvetti Correlation-Energy Formula into a Functional of the Electron Density. *Phys. Rev. B* **1988**, *37*, 785.
(34) Landau, L. D.; Lifshitz, E. M. *Theory of Elasticity*; Elsevier: Amsterdam, 1986.
(35) Gammon, P. H.; Kiefte, H.; Clouter, M. J.; Denner, W. W. Elastic Constants of Artificial and Natural Ice Samples by Brillouin Spectroscopy. *J. Glaciol.* **1983**, *29*, 433−460.
(36) Fletcher, N. H. *The Chemical Physics of Ice*; Cambridge Monographs on Physics: Cambridge, U.K., 1970.
(37) Penny, A. H. A. A Theoretical Determination of the Elastic Constants of Ice. *Math. Proc. Cambridge Philos. Soc.* **1948**, *44*, 423−439.
(38) Casazza, S.; Baima, J.; Mahmoud, A.; Kirtman, B. Ab initio Investigation of Electronic and Vibrational Contributions to Linear and Nonlinear Dielectric Properties of Ice. *J. Chem. Phys.* **2014**, *140*, 224702.
(39) Murray, É. D.; Galli, G. Dispersion Interactions and Vibrational Effects in Ice as a Function of Pressure: A First Principles Study. *Phys. Rev. Lett.* **2012**, *108*, 105502.
(40) Lu, D.; Gygi, F.; Galli, G. Dielectric Properties of Ice and Liquid Water from First-Principles Calculations. *Phys. Rev. Lett.* **2008**, *100*, 147601.
(41) Stuve, E. M. Ionization of Water in Interfacial Electric Fields: An Electrochemical Overview. *Chem. Phys. Lett.* **2012**, *519*−*520*, 1−17.
(42) Jaccard, C. Thermodynamics of Irreversible Processes Applied to Ice. *Phys. Kondens. Mater.* **1964**, *3*, 98−118.
(43) Schönherr, M.; Slater, B.; Hutter, J.; VandeVondele, J. Dielectric Properties of Water Ice, the Ice I_h/XI Phase Transition, and an Assessment of Density Functional Theory. *J. Phys. Chem. B* **2014**, *118*, 590−596.
(44) Hassanali, A.; Prakash, M. K.; Eshet, H.; Parrinello, M. On the Recombination of Hydronium and Hydroxide Ions in Water. *Proc. Natl. Acad. Sci. U. S. A.* **2011**, *108*, 20410−20415.
(45) Petrenko, V. F.; Whitworth, R. W. *Physics of Ice*; Oxford University Press: Oxford, U.K., 1999; p 72 for a list of referenced studies on the correlation parameter G of ice I_h.
(46) Maidique, M. A.; von Hippel, A.; Westphal, W. B. Transfer of protons through pure ice in single crystals - Part III. The dielectric relaxation spectra of water, ice, and aqueous solutions and their interpretation. Technical Report 8; Laboratory for Insulation Researc, Massachusetts Institute of Technology: Cambridge, MA, 1970.
(47) Liu, B.; Yang, J.; Wang, Q.; Han, Y.; Ma, Y.; Gao, C. Determination of Phase Diagram of Water and Investigation of Electrical Transport Properties of Ices VI and VII. *Phys. Chem. Chem. Phys.* **2013**, *15*, 14364−14369.
(48) Batista, E. R.; Xantheas, S. S.; Jónsson, H. Molecular Multipole Moments of Water Molecules in Ice I_h. *J. Chem. Phys.* **1998**, *109*, 4546.
(49) Ishii, F.; Terada, K.; Miura, S. First-Principles Study of Spontaneous Polarization and Water Dipole Moment in Ferroelectric Ice XI. *Mol. Simul.* **2012**, *38*, 369−372.
(50) Shevnukov, S. V.; Vegiri, A. Electric field induced transitions in water clusters. *J. Mol. Struct. (THEOCHEM)* **2002**, *593*, 19−32.